Desalination and Water Treatment
www.deswater.com

doi: 10.1080/19443994.2016.1195291

57 (2016) 28939–28946
December

Taylor & Francis
Taylor & Francis Group

Environmental remediation of Cr(VI) solutions using Ni-bismuth oxyiodide nanospheres

E.S. Baeissa

Faculty of Science, Chemistry Department, King Abdulaziz University, P.O. Box 80203, Jeddah 21589, Saudi Arabia, Tel. +966 6400000; Fax: +966 2 6952292; email: elhambaeissa@gmail.com

Received 24 January 2016; Accepted 24 May 2016

ABSTRACT

Bismuth oxyiodide (BiOI) nanospheres were prepared using a facile solvothermal method. Nickel was doped into the surface of the BiOI nanospheres using a photoassisted deposition method. Various characterization techniques, such as X-ray diffraction (XRD), PL, UV–vis, XRD, transmission electron microscope and BET surface area analyses, were used to characterize the BiOI nanosphere and Ni-BiOI nanosphere samples. The photocatalytic performance of the BiOI nanosphere and Ni-BiOI nanosphere samples was studied for the reduction of Cr(VI) to Cr(III) under visible light irradiation. The results indicated that the weight per cent of doped nickel plays an important role in controlling the band gap of bismuth oxyiodide and hindering the electron–hole recombination rate. The addition of nickel decreased the band gap from 2.7 to 2.16 eV due to a decrease in the weight per cent of nickel from zero to 0.8 wt%, respectively. In addition, the BET surface area of the BiOI nanospheres decreased from 145 to 128 m^2/g as the weight per cent of nickel increased from zero to 0.8 wt%, respectively, due to blockage of BiOI nanosphere pores and doping with nickel. The X-ray photoelectron spectroscopy results indicate that nickel was doped as metallic nickel. The 0.6 wt% Ni-BiOI nanosphere photocatalyst reduced Cr(VI) to Cr(III) within 30 min, and its photocatalytic activity reached 100%. In addition, this catalyst can be used five times without loss of its photocatalytic activity.

Keywords: Bismuth oxyiodide; Ni doping; Photocatalyst; Cr(VI) reduction

1. Introduction

Chromium exists in two oxidation states (i.e. chromium(VI) and chromium(III)). Chromium(VI) is more toxic, mobile and soluble than chromium(III) due to its ability to adsorb onto inorganic surfaces more easily. Due to the dangers of the presence of Cr ions in drinking water, chromium(VI) is considered to be a high priority hazard according to the United States EPA. The main sources of chromium(VI) are leather tanning, chromium electroplating and paint industries. Many efforts have attempted to convert chromium(VI) to chromium(III), which is one hundred times less mobile and less toxic. One of these approaches involves a reduction process where alkalization or neutralization of a chromium solution leads to the formation of $Cr(OH)_3$. In addition, further reduction leads to the formation of chromium metal [1,2]. Furthermore, different methods have been employed for the removal of chromium(VI) including electrolytic [3], ion exchange [4], freeze separation, reverse osmosis [5], solvent extraction [6], adsorption on activated charcoal [1], reduction followed by chemical precipitation [7] and reduction [8,9] methods. Each of these techniques has its own disadvantages including an inability to meet

health and hazards regulations, high energy consumption and highly toxic hazardous waste. The photocatalytic process can efficiently reduce chromium(VI) to chromium(III), and titanium dioxide is the most well-known photocatalyst due to its high stability, high photocatalytic activity and low cost. However, the use of titanium dioxide is hindered by two limitations. Titanium dioxide exhibits a large band gap, which leads to UV absorption. In addition, titanium dioxide possesses a high electron–hole recombination rate. Therefore, various methods have been used to shift the absorption from the UV region to the visible region and decrease the electron–hole recombination rate, which can be accomplished by metal or non-metal doping [10–22]. Bismuth oxyiodide is a p-type semiconductor with a narrow band gap. Therefore, this material exhibits excellent visible light absorption, which makes it a promising photocatalyst for the photocatalytic degradation of pollutants [23,24]. The disadvantages of bismuth oxyiodide for use as a commercial photocatalyst include a low BET surface area and rapid electron–hole recombination rate [23]. Many efforts have been focused on preventing electron–hole recombination [25–33]. BiOI/Bi_2O_3 composites have been prepared by Li et al. [34] who reported that the BiOI/Bi_2O_3 composites exhibit excellent photocatalytic activities for the degradation of 4-chlorophenol and phenol. AgI/BiOI composite photocatalysts were prepared by Cheng et al. [35] who reported that the addition of AgI to BiOI can control the electron–hole recombination rate. In addition, the composites exhibit excellent photocatalytic activities for the degradation of 4-chlorophenol. To the best of our knowledge, no previous studies have investigated the modification of bismuth oxyiodide via addition of nickel or the reduction of Cr(VI) by bismuth oxyiodide or nickel-bismuth oxyiodide. Therefore, the aim of this study was to prepare bismuth oxyiodide nanospheres with a high surface area using a facile solvothermal method and then control the electron–hole recombination rate by nickel doping. In addition, the photocatalytic performance of the bismuth oxyiodide and nickel-bismuth oxyiodide nanospheres was evaluated for the photocatalytic reduction of Cr(VI) under visible light irradiation.

2. Experimental

2.1. Preparation of photocatalysts

2.1.1. Preparation of BiOI nanospheres

Bismuth oxyiodide (BiOI) nanospheres were prepared using a facile solvothermal method. Typically, 1.5 mmol of cetyltrimethyl ammonium hydroxide were dispersed in 40 mL of ethylene glycol (EG) under magnetic stirring for 30 min. The mixture was ultrasonically treated for 1 h. Next, 1.5 mmol of Bi$(NO_3)_3{\cdot}5H_2O$ and 1.5 mmol of KI were added to this mixture followed by stirring for 30 min. Then, the resulting suspension was transferred into a 50-mL Teflon-lined stainless-steel autoclave and heated at 160˚C for 24 h. The final products were collected by centrifugation and washed with deionized water and absolute ethanol three times followed by drying at 80˚C for 8 h under vacuum.

2.1.2. Preparation of Ni-BiOI nanospheres

The different nickel metal contents (0.2, 0.4, 0.6 and 0.8 wt%) were doped into the surface of the bismuth oxyiodide nanospheres using a photoassisted deposition method. Briefly, the bismuth oxyiodide nanospheres were dispersed for 1 h in an aqueous solution of nickel nitrate, and then, the resulting mixture was irradiated with UV light (150 W) for 24 h. After filtering and washing, the resulting material was dried at 100˚C for 24 h followed by hydrogen reduction for 2 h at 120˚C.

2.2. Characterization techniques and apparatuses

The nanostructure morphology and sample dimensions were measured using a JEOL-JEM-1230 transmission electron microscope (TEM). The samples were suspended in ethanol and ultrasonicated for 30 m. A small amount of the sample was coated with carbon, dried on a copper grid and loaded into the TEM. To determine the surface area, the N_2-adsorption measurements were performed on treated samples (2 h under vacuum at 100˚C) using a Nova 2000 series Chromatech apparatus at 77 K. The crystalline phase was determined by powder X-ray diffraction (XRD) using a Bruker axis D8 with Cu Kα radiation (λ = 1.540 Å) at room temperature. X-ray photoelectron spectroscopy (XPS) measurements were performed on a Thermo Scientific K-ALPHA spectrometer. The band gap performance was determined by UV–vis diffuse reflectance spectroscopy (UV–vis-DRS), and the spectra were acquired using a UV–vis-NIR spectrophotometer (V-570, Jasco, Japan) in air at room temperature to detect the absorption over a range from 200 to 800 nm. The photoluminescence (PL) emission spectra were obtained with a Shimadzu RF-5301 fluorescence spectrophotometer.

2.3. Photocatalytic performance

The application of the synthesized nanoparticles for the photoreduction of chromium(VI) was studied

under UV irradiation. The experiments were performed using a horizontal cylinder annular batch reactor. The photocatalyst was irradiated using a xenon lamp (300 W). In a typical experiment, the desired catalyst amount was suspended in 500 mL of a 100 mg/L $K_2Cr_2O_7$ solution. The reaction was performed isothermally at 25°C, and samples of the reaction mixture were analysed at different time intervals for a total reaction time of 1 h. The concentration of chromium (VI) in the samples was estimated using a UV–vis spectrophotometer (V-570, JASCO, Japan) at 540 nm according the standard diphenylcarbazide method [36].

The photoreduction efficiency of chromium(VI) was measured by applying the following equation:

$$\% \text{ Photoreduction efficiency} = (C_o - C_t)/C_o \times 100$$

where C_o is the initial concentration of chromium(VI) in the solution at time zero and C_t is the concentration of chromium(VI) in the solution at time t.

3. Results and discussion

3.1. Characterizations of BiOI and Ni-BiOI nanospheres

The XRD patterns of the BiOI and Ni-BiOI samples are shown in Fig. 1. The results indicate that the BiOI and Ni-BiOI samples were primarily composed of bismuth oxyiodide. As the content of doped nickel increased, peak intensity decreased, and the peak width broadened. In addition, no peak was observed for nickel or nickel oxide in the patterns of the nickel-doped bismuth oxyiodide samples due to the nickel content being lower than the XRD detection limit or the nickel being well dispersed on the bismuth oxyiodide surface.

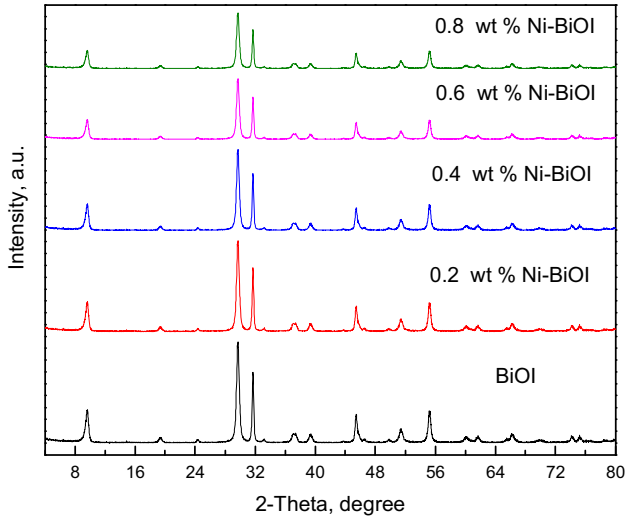

Fig. 1. XRD patterns of the BiOI and Ni-BiOI nanosphere samples.

The XPS spectra of Bi 4f (A), I 3d (B), O 1s (C) and Ni 2p (D) for the 0.6 wt% Ni-BiOI sample are shown in Fig. 2. The results indicate that the main Bi form is Bi^{3+} based on the Bi $4f_{7/2}$ and Bi $4f_{5/2}$ peaks at binding energies of 158.6 and 163.9 eV, respectively (Fig. 2(A)). The main I form is I^- based on the I $3d_{5/2}$ and I $3d_{3/2}$ peaks located at binding energies of 619.2 and 630.5 eV, respectively (Fig. 2(B)). The main O form is O^{2-} based on the O 1s peak at binding energy of 529.2 eV, as shown in Fig. 2(C). The Bi 4f, I 3d and O 1s XPS spectra confirm that the structure of bismuth oxyiodide is BiOI. This result is in agreement with the XRD results. In addition, the main Ni form is metallic nickel based on the Ni $2p_{3/2}$ and Ni $2p_{1/2}$ peaks at binding energies of 852.6 and 870.0 eV, respectively (Fig. 2(D)).

Fig. 3 shows the TEM images of BiOI and Ni-BiOI. These images indicate that BiOI is a nanosphere and nickel was doped as dots. The nickel dispersion on the bismuth oxyiodide surface was controlled by the doped nickel content. In addition, the doped nickel dispersion increased as the nickel content increased from 0 to 0.6 wt%, as shown in Fig. 3(A)–(D). A nickel content above 0.6 wt% increased the doped nickel aggregation, as shown in Fig. 3(E).

Table 1 shows the texture parameters of the BiOI and Ni-BiOI samples. The BET surface areas were 145, 139, 135, 130 and 128 m^2/g for BiOI, 0.2 wt% Ni-BiOI, 0.4 wt% Ni-BiOI, 0.6 wt% Ni-BiOI and 0.8 wt% Ni-BiOI, respectively. The total pore volumes of the Ni-BiOI samples were smaller than those of BiOI, which may be due to blockage of the BiOI pores due to metallic nickel doping.

Fig. 4 shows the UV–vis diffuse reflectance spectra of the BiOI and Ni-BiOI samples. The results demonstrate that the BiOI and Ni-BiOI samples absorb in the visible region, and the addition of nickel to BiOI shifts the absorption edges to longer wavelengths. In addition, the nickel content affects the absorption edge. The edge shifted to a longer wavelength as the nickel weight percentage content increased from 0 to 0.6. However, a nickel content higher than 0.6 did not significantly affect the absorption edge. Table 2 lists the BiOI and Ni-BiOI band gap values, which were calculated based on the UV–vis spectra. The band gap energy values were 2.70, 2.30, 2.25, 2.18 and 2.16 eV for BiOI, 0.2 wt% Ni-BiOI, 0.4 wt% Ni-BiOI, 0.6 wt% Ni-BiOI and 0.8 wt% Ni-BiOI, respectively. Therefore, the BiOI band gap can be controlled by the doped nickel content.

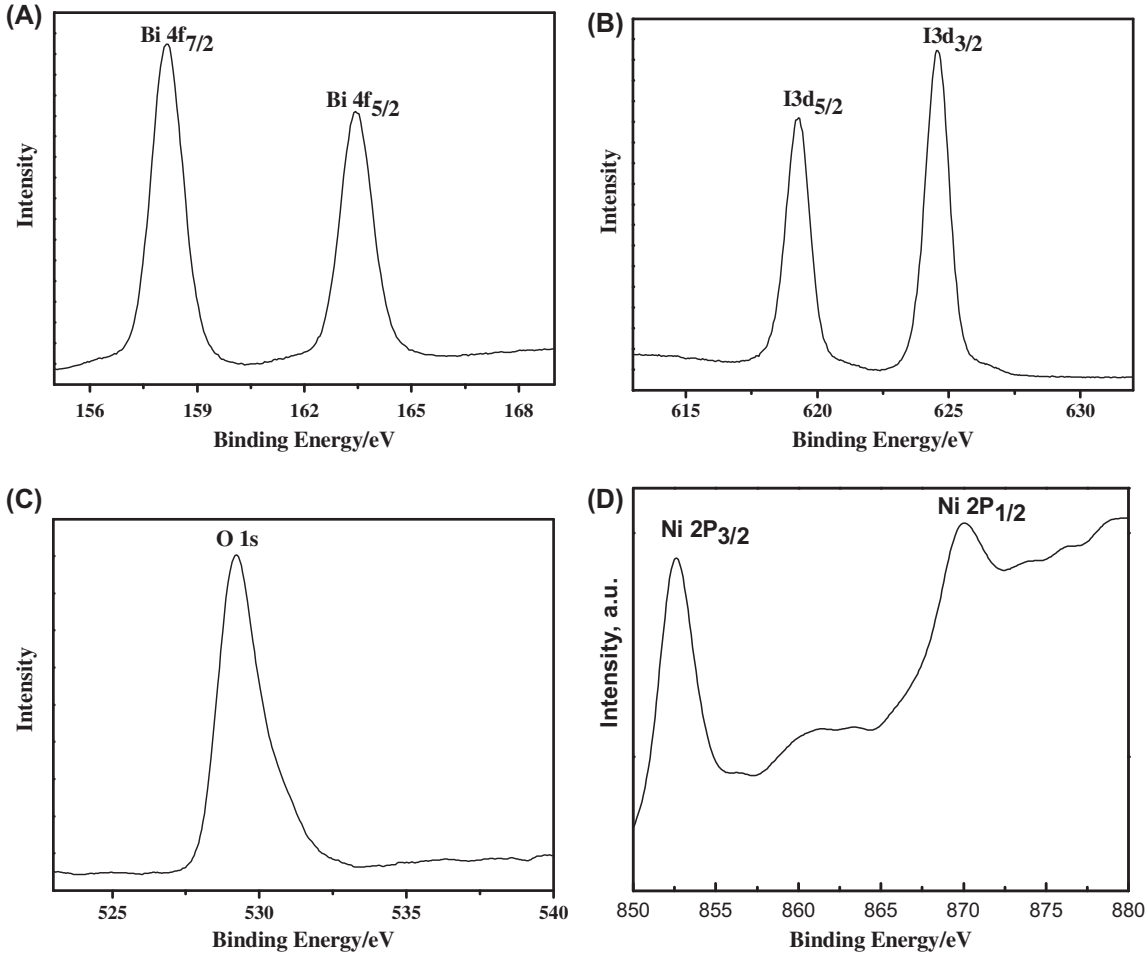

Fig. 2. XPS spectra of Bi 4f (A), I 3d (B), O 1s (C) and Ni 2p (D) for the 0.6 wt% Ni-BiOI sample.

Fig. 5 shows the PL spectra of the BiOI and Ni-BiOI samples. The results indicate that the BiOI PL peak intensity decreased as the metallic nickel content increased from 0.0 to 0.6. A metallic nickel content higher than 0.6 did not significantly affect the PL peak intensity. Therefore, the nickel content affects the electron–hole recombination rate.

3.2. *Photocatalytic activities of the BiOI and Ni-BiOI nanospheres samples*

The effect of the Ni content on the photocatalytic activity of the BiOI and Ni-BiOI nanosphere samples for the reduction of Cr(VI) is shown in Fig. 6. The photocatalytic conditions are 60 min reaction time; 0.4 g/L photocatalyst dose; 100 ppm chromium concentration. The photocatalytic reactions were carried out under the following conditions: 75 ppm $K_2Cr_2O_7$ solution, 500 ml of $K_2Cr_2O_7$ and 0.4 g/l photocatalyst dose. The results reveal that the BiOI photocatalyst has a very low photocatalytic activity (48%), and doping BiOI with metallic nickel increased the photocatalytic activity. In addition, an increase in the doped nickel content from 0 to 0.6 wt% increased the photocatalytic activity from 48 to 100%, respectively. The photocatalytic activity remained unchanged when the doped nickel content was higher than 0.6 wt%. To confirm the photocatalytic reduction of Cr(VI) to Cr (III) by the 0.6 wt% Ni-BiOI sample, the XPS spectra of the Cr 2p level for the 0.6 wt% Ni-BiOI sample was measured after the photocatalytic reaction (Fig. 7). The results indicate that the 0.6 wt% Ni-BiOI photocatalyst that reduced Cr(VI) to Cr(III) exhibited two peaks at 576.8 and 586.5 eV corresponding to Cr $2p_{3/2}$ and Cr $2p_{1/2}$, respectively.

Fig. 8 shows the effect of the 0.6 wt% Ni-BiOI photocatalyst dose on the photocatalytic activity of BiOI for Cr(VI) photocatalytic reduction. The photocatalytic conditions are 60 min reaction time; 0.6 wt% Ni-BiOI used photocatalyst; 100 ppm chromium concentration.

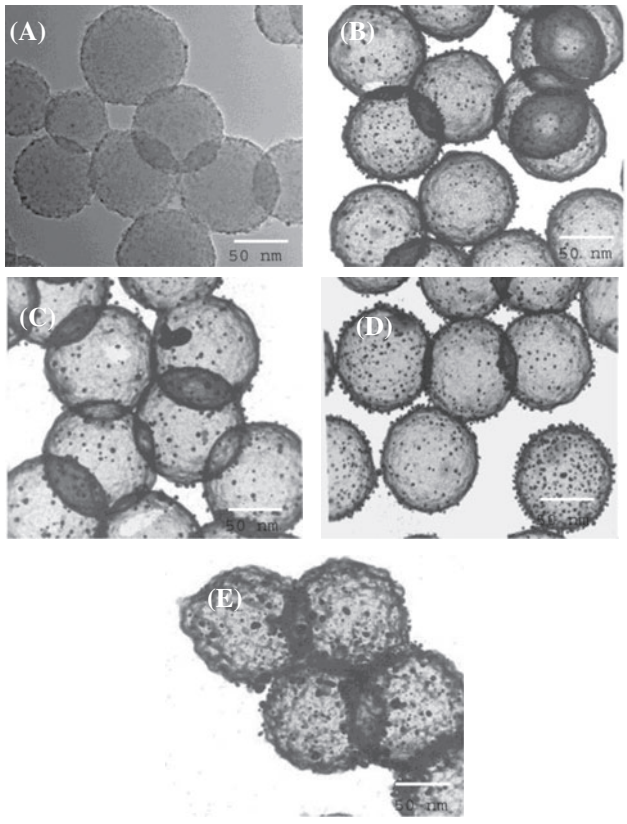

Fig. 3. TEM images of the BiOI and Ni-BiOI nanosphere samples, where the wt% of Ni was 0.0 (A), 0.2 (B), 0.4 (C), 0.6 (D) and 0.8 (E).

Table 1
BET surface area and total pore volume of the BiOI and Ni-BiOI samples

Sample	S_{BET} (m^2/g)	Total pore volume (cm^3/g)
BiOI	145.0	0.0700
0.2 wt% Ni-BiOI	139.0	0.0650
0.4 wt% Ni-BiOI	135.0	0.0600
0.6 wt% Ni-BiOI	130.0	0.0550
0.8 wt% Ni-BiOI	128.0	0.0500

The results reveal that an increase in the photocatalyst dose from 0.2 to 0.4 g/L increased the photocatalytic activity from 70 to 100%. The reaction time required to complete the Cr(VI) photocatalytic reduction decreased from 60 to 50 to 30 min as the photocatalyst dose increased from 0.4 to 0.6 to 0.8 g/L, respectively. This result was due to an increase in the photocatalyst dose which increased the number of active photocatalytic sites available for photocatalytic reduction. In addition, the reaction time required for complete Cr(VI)

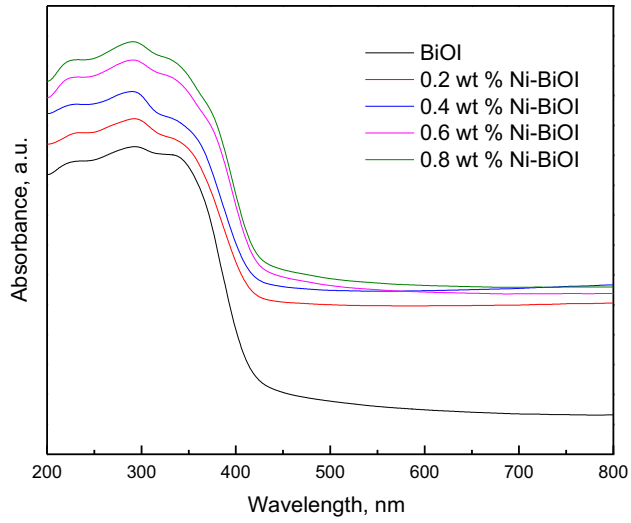

Fig. 4. UV–vis absorption spectra of the BiOI and Ni-BiOI nanosphere samples.

Table 2
Band gap energy of the BiOI and Ni-BiOI nanospheres

Sample	Band gap energy (eV)
BiOI	2.70
0.2 wt% Ni-BiOI	2.30
0.4 wt% Ni-BiOI	2.25
0.6 wt% Ni-BiOI	2.18
0.8 wt% Ni-BiOI	2.16

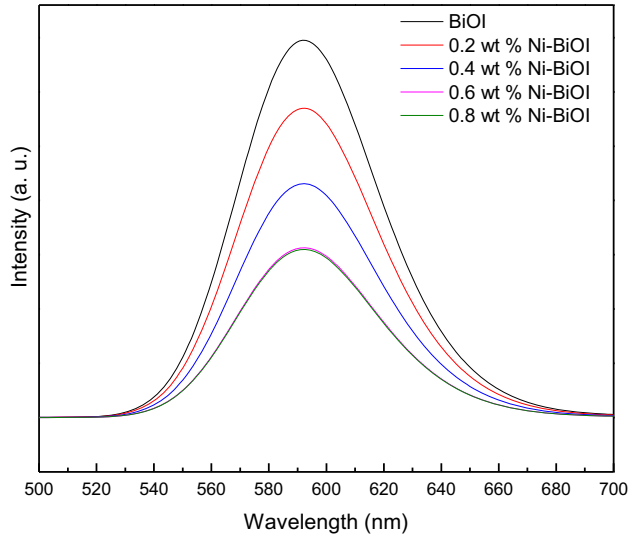

Fig. 5. PL spectra of the BiOI and Ni-BiOI nanosphere samples.

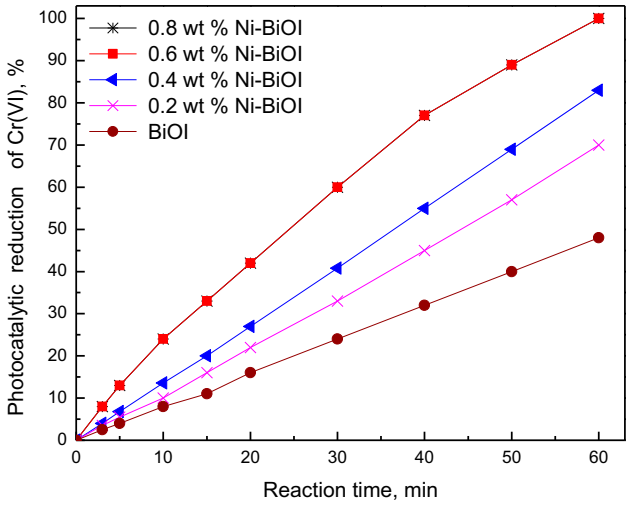

Fig. 6. Effect of the wt% of Ni on the photocatalytic activity of the BiOI and Ni-BiOI nanosphere samples for the reduction of Cr(VI).

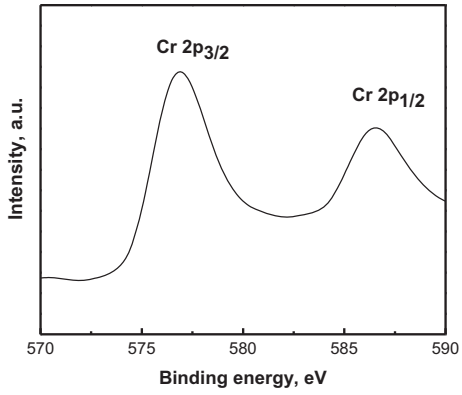

Fig. 7. XPS spectra of Cr 2p for the 0.6 wt% Ni-BiOI sample after being used for the reduction of a Cr(VI) solution.

photocatalytic reduction increased to 40 min when the photocatalyst dose increased above 1.0 g/L. This trend was due to photocatalyst doses higher than 1.0 g/L hindering light penetration to the photocatalyst surface, decreasing the photocatalytic activity and increasing the reaction time.

Fig. 9 shows the effect of the initial Cr(VI) concentration on the photocatalytic activity of the 0.6 wt% Ni-BiOI photocatalyst for Cr(VI) photocatalytic reduction. The photocatalytic conditions are 60 min reaction time; 0.6 wt% Ni-BiOI used photocatalyst; 0.8 g/L photocatalyst dose. The results indicate that the photocatalytic activity of the 0.6 wt% Ni-BiOI photocatalyst remained relatively constant as the initial Cr(VI) concentration increased from 25 to 50 ppm. However, the

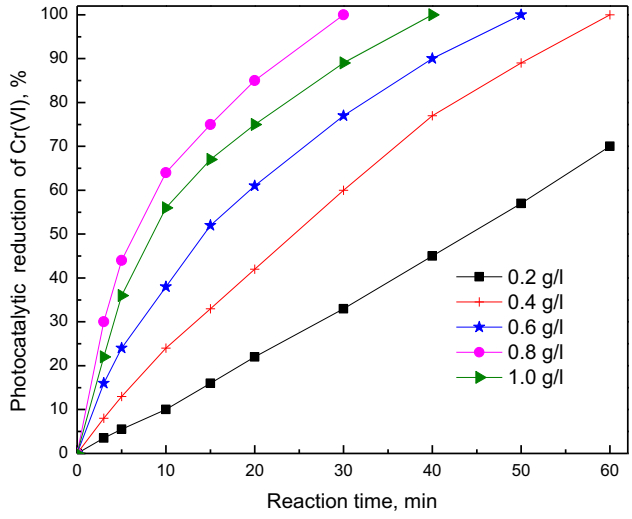

Fig. 8. Effect of the photocatalyst dose of the 0.6 wt% Ni-BiOI sample on the photocatalytic reduction of a Cr(VI) solution.

photocatalytic activity decreased from 100 to 58% when the initial Cr(VI) concentration was increased from 50 to 175 ppm after 20 min, respectively.

Fig. 10 shows the results from the reuse of the 0.6 wt% Ni-BiOI photocatalyst for Cr(VI) photocatalytic reduction. The photocatalytic conditions has 30 min reaction time; 0.6 wt% Ni-BiOI used photocatalyst; 100 ppm chromium concentration; 0.8 g/L photocatalyst dose. The results indicate that the 0.6 wt% Ni-BiOI photocatalyst exhibited a high photocatalytic stability after being reused five times.

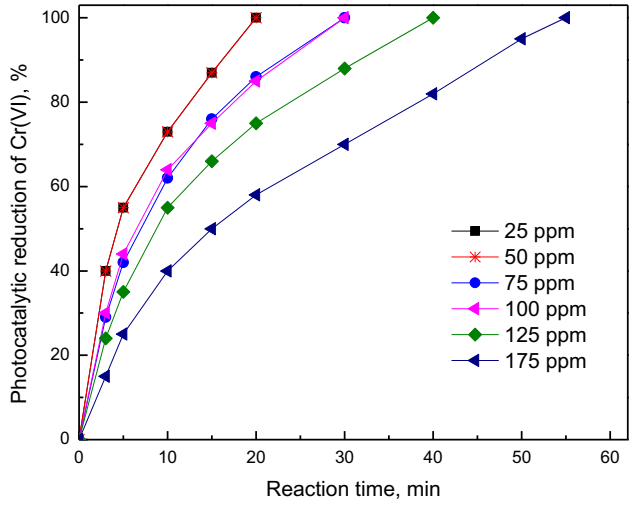

Fig. 9. Effect of the initial Cr(VI) solution concentration on the photocatalytic reduction of a Cr(VI) solution.

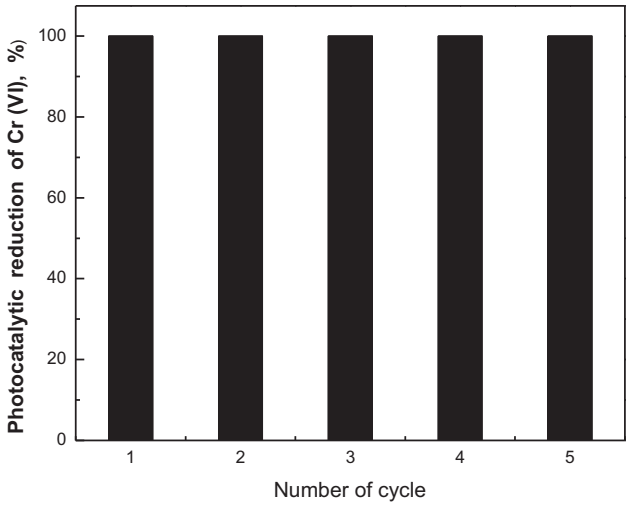

Fig. 10. Recycling and reuse of the photocatalysts for the photocatalytic reduction of a Cr(VI) solution.

4. Conclusions

Bismuth oxyiodide were prepared using a facile solvothermal method, and nickel metal was doped onto the bismuth oxyiodide nanospheres via a photoassisted deposition method. The nickel-doped bismuth oxyiodide nanospheres exhibited a high photocatalytic activity under visible light irradiation and are a promising photocatalyst. Nickel doping of the bismuth oxyiodide nanospheres resulted in a shift in the bismuth oxyiodide absorption edges to a longer wavelength. The XPS results indicate that the doped nickel was present as metallic nickel. The 0.6 wt% Ni-BiOI photocatalyst was the most active photocatalyst. About 100% Cr(VI) photocatalytic reduction was achieved using the 0.6 wt% Ni-BiOI photocatalyst under the following conditions: a 0.8 g/L photocatalyst dose, 100 ppm Cr(VI) concentration and 30 min reaction time. The 0.6 wt% Ni-BiOI nanosphere photocatalyst exhibited high photocatalytic stability after being reused five times.

References

[1] F. Melak, G.D. Laing, A. Ambelu, E. Alemayehu, Application of freeze desalination for chromium(VI) removal from water, Desalination 377 (2016) 23–27.
[2] Z. An, H. Zhang, Q. Wen, Z. Chen, M. Du, Desalination combined with hexavalent chromium reduction in a microbial desalination cell, Desalination 354 (2014) 181–188.
[3] S.D. Kim, K.S. Park, M.B. Gu, Toxicity of hexavalent chromium to *Daphnia magna*: Influence of reduction reaction by ferrous iron, J. Hazard. Mater. 93(2) (2002) 155–164.
[4] Z. Yao, Y. Li, Y. Cui, K. Zheng, B. Zhu, H. Xu, L. Zhu, Tertiary amine block copolymer containing ultrafiltration membrane with pH-dependent macromolecule sieving and Cr(VI) removal properties, Desalination 355 (2015) 91–98.
[5] A. Padilla, E.L. Tavani, Treatment of an industrial effluent by reverse osmosis, Desalination 126(1–3) (1999) 219–226.
[6] S. Rengaraj, C.K. Joo, Y. Kim, J. Yi, Kinetics of removal of chromium from water and electronic process wastewater by ion exchange resins: 1200H, 1500H and IRN97H, J. Hazard. Mater. 102(2–3) (2003) 257–275.
[7] A. Özer, H.S. Altundoğan, M. Erdem, F. Tümen, A study on the Cr(VI) removal from aqueous solutions by steel wool, Environ. Pollut. 97(1–2) (1997) 107–112.
[8] E. Gkika, A. Troupis, A. Hiskia, E. Papaconstantinou, Photocatalytic reduction of chromium and oxidation of organics by polyoxometalates, Appl. Catal. B: Environ. 62 (2006) 28–34.
[9] A.K. Tripathi, M.C. Mathpal, P. Kumar, M.K. Singh, M.A.G. Soler, A. Agarwal, Structural, optical and photoconductivity of Sn and Mn doped TiO_2 nanoparticles, J. Alloys Compd. 622 (2015) 37–47.
[10] R.M. Mohamed, E.S. Baeissa, Mordenite encapsulated with Pt–TiO_2: Characterization and applications for photocatalytic degradation of direct blue dye, J. Alloys Compd. 558 (2013) 68–72.
[11] R.M. Mohamed, UV-assisted photocatalytic synthesis of TiO_2-reduced graphene oxide with enhanced photocatalytic activity in decomposition of sarin in gas phase, Langmuir 50 (2012) 147–156.
[12] W. Shu, Y. Liu, Z. Peng, K. Chen, C. Zhang, W. Chen, Synthesis and photovoltaic performance of reduced graphene oxide–TiO_2 nanoparticles composites by solvothermal method, J. Alloys Compd. 563 (2013) 229–233.
[13] H. Yan, S.T. Kochuveedu, L.N. Quan, S.S. Lee, D.H. Kim, Enhanced photocatalytic activity of C, F-codoped TiO_2 loaded with AgCl, J. Alloys Compd. 560 (2013) 20–26.
[14] Y. Cao, Z. Zhao, J. Yi, C. Ma, D. Zhou, R. Wang, C. Li, J. Qiu, Luminescence properties of Sm^{3+}-doped TiO_2 nanoparticles: Synthesis, characterization, and mechanism, J. Alloys Compd. 554 (2013) 12–20.
[15] R.M. Mohamed, E.S. Aazam, H_2 production with Low CO selectivity from photocatalytic reforming of glucose on Ni/TiO_2–SiO_2, Chin. J. Catal. 33 (2012) 247–253.
[16] R.M. Mohamed, E.S. Aazam, Preparation and characterization of platinum doped porous titania nanoparticles for photocatalytic oxidation of carbon monoxide, J. Alloys Compd. 509 (2011) 10132–10138.
[17] H. Zhang, C. Liang, J. Liu, Z. Tian, G. Wang, W. Cai, Defect-mediated formation of Ag cluster-doped TiO_2 nanoparticles for efficient photodegradation of pentachlorophenol, Langmuir 28 (2012) 3938–3944.
[18] R. Liu, P. Wang, X. Wang, H. Yu, J. Yu, UV- and visible-light photocatalytic activity of simultaneously deposited and doped Ag/Ag(I)–TiO_2 photocatalyst, J. Phys. Chem. C 116 (2012) 17721–17728.
[19] R.M. Mohamed, E.S. Aazam, Characterization and catalytic properties of nano-sized Au metal catalyst on Titanium containing high mesoporous silica (Ti-HMS) synthesized by photo-assisted deposition and impregnation methods, Catal. Commun. V2011 (2011) 7 p (Article ID 137328).

[20] R.M. Mohamed, I.A. Mkhalid, Characterization and catalytic properties of nano-sized Ag metal catalyst on TiO_2–SiO_2 synthesized by photo-assisted deposition and impregnation methods, J. Alloys Compd. 501 (2010) 301–306.
[21] K. Chen, X. Feng, R. Hu, Y. Li, K. Xie, Y. Li, H. Gu, Effect of Ag nanoparticle size on the photoelectrochemical properties of Ag decorated TiO_2 nanotube arrays, J. Alloys Compd. 554 (2013) 72–79.
[22] R.M. Mohamed, I.A. Mkhalid, The effect of rare earth dopants on the structure, surface texture and photocatalytic properties of TiO_2–SiO_2 prepared by sol–gel method, J. Alloys Compd. 501 (2010) 143–147.
[23] X. Xiao, W.D. Zhang, Facile synthesis of nanostructured BiOI microspheres with high visible light-induced photocatalytic activity, J. Mater. Chem. 20 (2010) 5866–5870.
[24] W.D. Wang, F.Q. Huang, X.P. Lin, J.H. Yang, Visible-light-responsive photocatalysts xBiOBr-(1 − x)BiOI, Catal. Commun. 9 (2008) 8–12.
[25] J. Henle, P. Simon, Nanosized BiOX (X = Cl, Br, I) particles synthesized in reverse microemulsions, Chem. Mater. 19 (2007) 366–373.
[26] L.J. Zhao, X.C. Zhang, C.M. Fan, Z.H. Liang, P.D. Han, First-principles study on the structural, electronic and optical properties of BiOX (X = Cl, Br, I) crystals, Phys. B: Condensed Matter 407 (2012) 3364–3370.
[27] X. Zhang, Z.H. Ai, F.L. Jia, L.Z. Zhang, Generalized one-pot synthesis, characterization, and photocatalytic activity of hierarchical BiOX (X = Cl, Br, I) nanoplate microspheres, J. Phys. Chem. C 112(3) (2008) 747–753.
[28] L.F. Zhu, C. He, Y.L. Huang, Z.H. Chen, D.H. Xia, M.H. Su, Y. Xiong, S.Y. Li, D. Shu, Enhanced photocatalytic disinfection of *E. coli* 8099 using Ag/BiOI composite under visible light irradiation, Sep. Purif. Technol. 91 (2012) 59–66.
[29] J. Cao, B.Y. Xu, H.L. Lin, B.D. Luo, S.F. Chen, Chemical etching preparation of BiOI/BiOBr heterostructures with enhanced photocatalytic properties for organic dye removal, Chem. Eng. J. 185–186 (2012) 91–99.
[30] T.B. Li, G. Chen, C. Zhou, Z.Y. Shen, R.C. Jin, J.X. Sun, New photocatalyst BiOCl/BiOI composites with highly enhanced visible light photocatalytic performances, Dalton Trans. 40 (2011) 6751–6758.
[31] X. Zhang, L.Z. Zhang, T.F. Xie, D.J. Wang, Low-temperature synthesis and high visible-light-induced photocatalytic activity of BiOI/TiO_2 heterostructures, J. Phys. Chem. C 113 (2009) 7371–7378.
[32] Y.R. Jiang, S.Y. Chou, J.L. Chang, S.T. Huang, H.P. Lin, C.C. Chen, Hydrothermal synthesis of bismuth oxybromide–bismuth oxyiodide composites with high visible light photocatalytic performance for the degradation of CV and phenol, RSC Adv. 5 (2015) 30851–30860.
[33] W.W. Lee, C.S. Lu, C.W. Chuang, Y.J. Chen, J.Y. Fu, C.W. Siao, C.C. Chen, Synthesis of bismuth oxyiodides and their composites: Characterization, photocatalytic activity, and degradation mechanisms, RSC Adv. 5 (2015) 23450–23463.
[34] Y.Y. Li, J.S. Wang, H.C. Yao, L.Y. Dang, Z.J. Li, Chemical etching preparation of BiOI/Bi_2O_3 heterostructures with enhanced photocatalytic activities, Catal. Commun. 12 (2011) 660–664.
[35] H.F. Cheng, W.J. Wang, B.B. Huang, Z.Y. Wang, J. Zhan, X.Y. Qin, X.Y. Zhang, Y. Dai, Tailoring AgI nanoparticles for the assembly of AgI/BiOI hierarchical hybrids with size-dependent photocatalytic activities, J. Mater. Chem A 1(24) (2013) 7131–7136.
[36] V. Maheswari, N. Balasubramanian, Spectrophotometric determination of chromium, based on ion-pair formation, Chern. Anal. (Warsaw) 41 (1996) 569–477.